ELSEVIER

Infrared Physics & Technology 42 (2001) 259–265

INFRARED PHYSICS & TECHNOLOGY

www.elsevier.com/locate/infrared

Space charge spectroscopy of integrated quantum well infrared photodetector–light emitting diode

M. Ershov [a,*], B. Yaldiz [a], A.G.U. Perera [a], S.G. Matsik [a], H.C. Liu [b], M. Buchanan [b], Z.R. Wasilewski [b], M.D. Williams [c]

[a] *Department of Physics and Astronomy, Georgia State University, Atlanta, GA 30303, USA*
[b] *Institute for Microstructural Sciences, National Research Council, Ottawa, Ontario, Canada K1A 0R6*
[c] *Department of Physics, Clark Atlanta University, Atlanta, GA 30314, USA*

Abstract

We present the results of the space charge spectroscopy of integrated quantum well infrared photodetector – light emitting diode (QWIP-LED). Quasistatic capacitance–voltage (C–V) characteristics under reverse bias display a step-like behavior due to a step-wise extension of the space charge region with bias. The parameters of the steps, and the frequency dispersion of the capacitance are used to determine the QW period thickness, QW doping level, and the number of QW periods. Measurement of the QWIP-LED admittance at various temperatures is used to obtain the QW activation energy and the conduction band offset.

Keywords: Quantum-well infrared photodetector; Light-emitting diode; Space charge spectroscopy; C–V characteristics; Admittance spectroscopy

1. Introduction

Recently proposed [1,2] integrated quantum well infrared photodetector–light emitting diode (QWIP-LED) is based on the principle of direct injection of carriers photoexcited in a QWIP by mid- or far-infrared radiation into LED active region and subsequent emission of near-infrared or visible radiation (see Fig. 1). Large area QWIP-LEDs are promising for infrared imaging, since they provide the upconversion of the incoming far-infrared image into a near-infrared output image, which can be easily read out using commercial CCD devices. Small lateral smearing of the upconverted image [3] and high efficiency of near-infrared LEDs guarantee potentially high quality and inexpensive infrared imagers. Integrated devices with both p-type and n-type QWIPs have been demonstrated [4,5], and the search for the optimum QWIP-LED imager design is still under way [6,7].

Under normal operating conditions the QWIP-LED is biased in the forward direction, i.e. the p–n junction of the LED is open, and the current is limited by the QWIP (see Fig. 1(b) and Fig. 2). Under reverse bias (Fig. 1(a)), the current in the QWIP-LED is blocked by the p–n junction, so that all applied voltage drops across the LED and a small part of the QWIP adjacent to the LED. The

* Corresponding author. Tel.: +1-404-651-2841; fax: +1-404-651-1427.
E-mail address: mershov@gsu.edu (M. Ershov).

1350-4495/01/$ - see front matter
PII: S1350-4495(01)00084-6

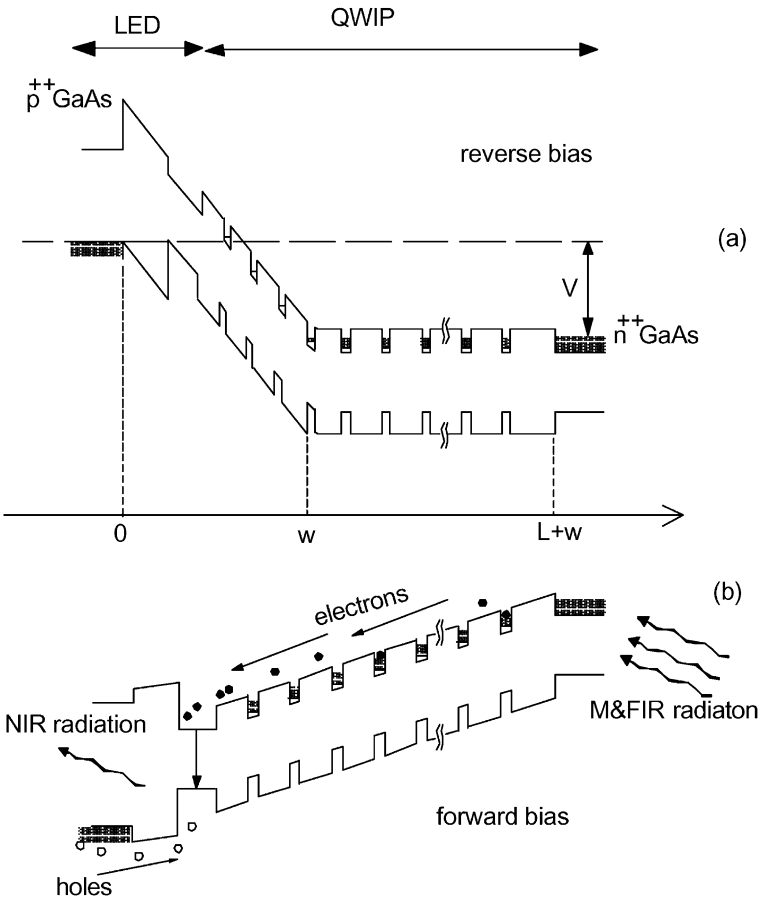

Fig. 1. Schematic band diagram of the QWIP-LED under (a) reverse and (b) forward bias voltage.

rest of the QWIP superlattice experiences zero electric field. The boundary of the space charge region on the QWIP side coincides with the position of QW, so by changing the applied voltage we can probe the recharging dynamics of the QWs, transport in the QW structure, and extract important physical information from these data. Thus, a reverse biased QWIP-LED is ideally suited for space charge spectroscopy.

Space charge spectroscopy is a powerful technique allowing non-destructive characterization of semiconductor microstructures. There are several versions of this technique, probing various transport and recharging regimes: (1) capacitance–voltage (C–V) profiling [8], (2) admittance spectroscopy [9–12], and (3) large signal transient spectroscopy [13,14]. All these approaches require negligibly small DC current level in the device. In the present work, we use C–V measurements and admittance (capacitance and conductance versus frequency) measurements to characterize QWIP-LEDs. We obtain the following parameters of the QW structure from the charge spectroscopy measurements: QW ionization energy, conduction band offset, thickness of the QW period, doping level of the QWs, and the number of the QW periods in QWIP.

2. Quantum well infrared photodetector – light emitting diode structure and measurement setup

The layer sequence of the QWIP-LED studied in this work is similar to that described earlier [6].

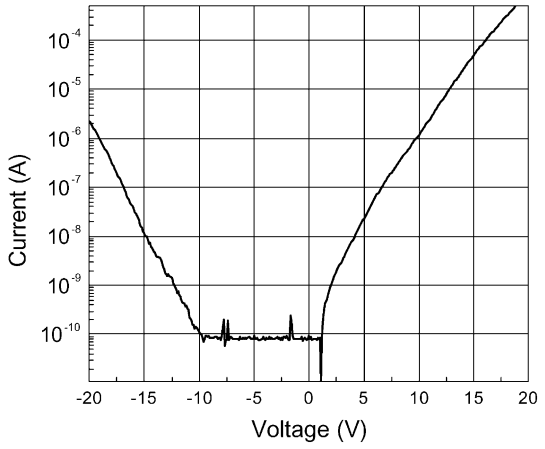

Fig. 2. Dark current voltage characteristic of the QWIP-LED at $T = 77$ K. Space charge spectroscopy is performed under reverse bias voltage where the DC current is small (-10 V $< V < 0$ V).

The LED was grown on the top of the QWIP. The QWIP consisted of the following layers (in growth sequence): a bottom contact layer of 1000 Å n-GaAs doped with Si at 2.5×10^{18} cm^{-3} grown on N^+ substrate, a 20 Å GaAs spacer, and 40 more GaAs/$Al_{0.45}Ga_{0.55}As$ quantum wells with a 300 Å barrier and 40 Å well. The wells were delta-doped with Si at $\Sigma = 7 \times 10^{11}$ cm^{-2}. These δ-spikes were positioned away from the well center towards the substrate by $\approx$10 Å to counterbalance the Si segregation during growth and ensure the symmetry of the QWIP structure. Growth continued with the following LED layers: an 800 Å $Al_xGa_{1-x}As$ layer graded from $x = 0.45$–0.10, a 300 Å $In_{0.02}Ga_{0.98}As$ well, a 400 Å $Al_xGa_{1-x}As$ layer graded from $x = 0.10$ to 0.26, a 400 Å $Al_{0.26}Ga_{0.74}As$ layer with its Be doping increased from 1.3×10^{18} to 3×10^{18} cm^{-3}, 400 Å p^{++} $Al_{0.26}Ga_{0.74}As$ layer doped at 10^{19} cm^{-3}, a 1000 Å p^{++} GaAs top contact layer doped at 1.3×10^{19} cm^{-3}, and finally a 1000 Å p^{++} GaAs top contact layer doped at 4×10^{19} cm^{-3}. The area of the QWIP-LED was $A = 400 \times 400$ μm^2. A schematic band diagram of the n-type QWIP-LED is shown in Fig. 1. The capacitance and conductance measurements were performed using an HP4284A LCR meter (1 kHz–1 MHz). I–V measurements were carried out using 2400 Keithley sourcemeter. Both capacitance and conductance of the QWIP-LED were recorded at various temperatures as functions of frequency. The amplitude of the modulating signal was 5 mV. The sample was mounted in a continuous flow cryostat where temperature can be controlled in the range 2.5–300 K using 9620-1 SI temperature controller. The temperature of the sample were measured with an accuracy of 0.5 K.

2.1. Quasistatic C–V characteristics

Fig. 2 shows the dark current I–V characteristic at temperature $T = 77$ K. The forward bias characteristic is typical for a QWIP, since the resistance of p–n junction is very low and conduction is limited by the QWIP. Under reverse bias, the p–n junction blocks the DC current, so the current is very low. At large reverse bias ($|V| > 10$ V) the breakdown of the p–n junction gives rise to a rapid increase in the current. Thus, the region of voltage -10 V $< V < 0$ V is suitable for the space charge spectroscopy measurements.

QWIP-LED displays a large negative capacitance under forward bias at low frequencies. This should be expected, since the conduction of the QWIP-LED under forward bias conditions is determined by the QWIP, and capacitance of QWIPs at low measurement frequency is typically negative [15,16].

Fig. 3 shows the C–V characteristics of the QWIP-LED measured at various frequencies at temperature $T = 300$ K. At low frequencies, the capacitance is determined by the depletion layer capacitance $C_0 = \varepsilon A/W$, where ε is the dielectric permittivity, and W is the depletion layer width (see Fig. 1(a)).

Capacitance decreases with increasing reverse bias due to the increase of the depletion layer width. However, the decrease in capacitance is not monotonic and displays a series of steps. These steps are explained as follows [17,18]. Under zero bias, the first QW in the QWIP next to the LED is partially depleted by electrons. The space charge region between n- and p-doped contacts spans from the heavily doped LED contact to the first QW in QWIP. The rest of the QW structure (“base”) is under zero electric field, since the DC current is zero and the Fermi level, determined by the QWIP doped contact, is constant. With the

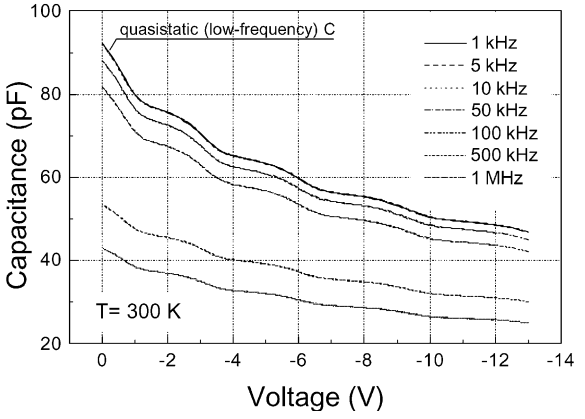

Fig. 3. Capacitance voltage characteristics measured at various frequencies for $T = 300$ K. The steps are related to the depletion of the QWs, as explained.

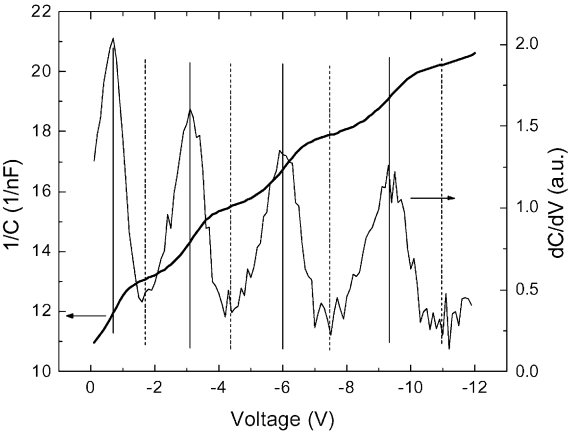

Fig. 4. Inverse capacitance and capacitance derivative dC/dV. The peaks of dC/dV curve correspond to step-wise extension of the depletion region between neighboring QWs after complete depletion of the QW by electrons. The minimums of dC/dV correspond to constant capacitance when the depletion layer edge coincides with a QW.

increase of negative voltage, the electric field in the space charge region is increased, and the electrons are pushed out of the first QW. All other QWs in the QWIP remain electrically neutral. When all electrons are depleted from the first QW, the boundary of the space charge region jumps to the second QW, so the width of the space charge region is increased by L_p, where L_p is the period of the QW structure. This corresponds to a step-like increase of the inverse capacitance by $\Delta(1/C) = L_p/(\varepsilon A)$. With increase of the reverse voltage, the boundary of the space charge region is fixed at the second QW, until this QW is completely depleted. The process of step-like extension of the space charge region repeats with further increase of bias. The ith step on the C–V characteristic is related to the depletion of the ith QW in QWIP.

The analysis presented above is based on the assumption that the boundary of space charge region in the LED heavily doped p^+ contact is fixed, and the space charge region extends towards QWIPs n^+ contact. This assumption is justified, since the 3D doping in the p^+ contact ($\sim 3 \times 10^{18}$ cm^{-3}) is much higher than effective 3D doping in QWIP $N_{\text{eff}} = e\Sigma/L_p \approx 2 \times 10^{17}$ cm^{-3}.

Fig. 4 illustrates the voltage dependence of the inverse capacitance and capacitance derivative dC/dV. It can be seen that the steps in the $1/C$ versus V plot are equidistant along the $1/C$ axis. The peaks of the capacitance derivative correspond to voltages at which the boundary QW is completely depleted and the space charge region jumps to the next QW. It can be shown from electrostatics considerations that the voltage offset between the positions of dC/dV peaks is given by $V_i - V_{i-1} = e\Sigma A/C_i$, where V_i is the voltage corresponding to a complete depletion of the ith QW, Σ is the 2D doping density of the QWs, and C_i is the low-frequency capacitance of the QWIP-LED when the boundary of the space charge region is located at the ith QW. Capacitance C_i corresponds to a voltage at which dC/dV curve has a minimum (Fig. 4).

From the distance between the steps along the $1/C$ axis we obtain the value of the QW period thickness as $L_p = 420 \pm 10$ Å. This value is within the $\sim$20% error of the design parameter $L_p = 340$ Å. The distances between the steps along the voltage axis allow the calculation of the QW doping density $\Sigma = (7.35 \pm 0.05) \times 10^{11}$ cm^{-2}. A better than 95% agreement between the extracted value of the doping density (7.35×10^{11} cm^{-2}) and the design parameter (7×10^{11} cm^{-2}) is obtained.

At higher measurement frequencies, there is not enough time for recharging of the boundary QW, so the space charge region spreads over to

the base region. As a result, the capacitance of the QWIP-LED decreases (see Fig. 3). In the high-frequency limit, QWs in the QWIP are not recharging upon application of a small-signal AC voltage, so the QWIP-LED capacitance becomes constant and equal to the geometric capacitance, i.e. to the parallel-plate capacitance between the heavily doped contacts on the LED and QWIP side (see Fig. 5(a)). The ratio of the inverse low-frequency capacitance of the QWIP base region determined experimentally to the inverse capacitance step gives 35 QW periods in the QWIP, close to the design value $N = 40$. Of course, the number of the QW periods in this QWIP-LED is 40, and the error $\sim$10% between the extracted number of the QW periods and the actual number of periods is due to the simplifications in our analysis.

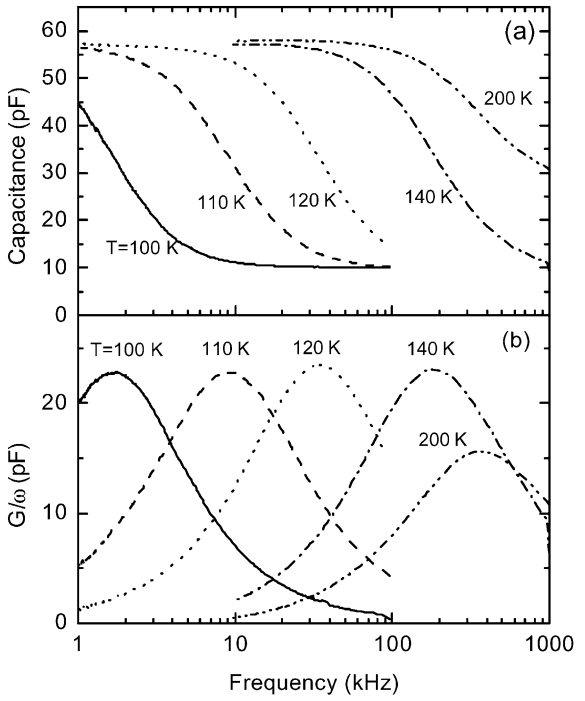

Fig. 5. Frequency dependence of (a) capacitance and (b) conductance (normalized by frequency) at various temperatures. The peaks of G/ω characteristics correspond to maximums of the capacitance derivative $dC/d(\log \omega)$. Temperature variation of the peak frequency is used to obtain the QW activation energy.

2.2. Admittance of QW structure

We have developed a theory of admittance of multiple QW structure with a blocking injection contact, which will be published elsewhere [19]. It shows that the QWIP-LED admittance can be represented by an equivalent circuit shown in the inset of Fig. 6. This circuit differs from the conventional one [20] by the presence of an additional resistance R_{QW}, which we call the QW resistance. The conventional model for admittance of a multiple QW structure assumes that under the small-signal AC excitation, only one (boundary) QW is recharged, and that recharging current is provided by the multiple QW structure, assuming that its conductivity is equal to the steady-state conductivity. In other words, it was assumed that the QW recharging processes are much faster than the carrier transport in the multiple QW structure. Our analysis shows, however, that under AC excitation the current can be limited either by the conductivity of the QW region, or by the QW recharging, depending on the physical parameters of the structure. The parameters of the equivalent circuit are expressed as follows:

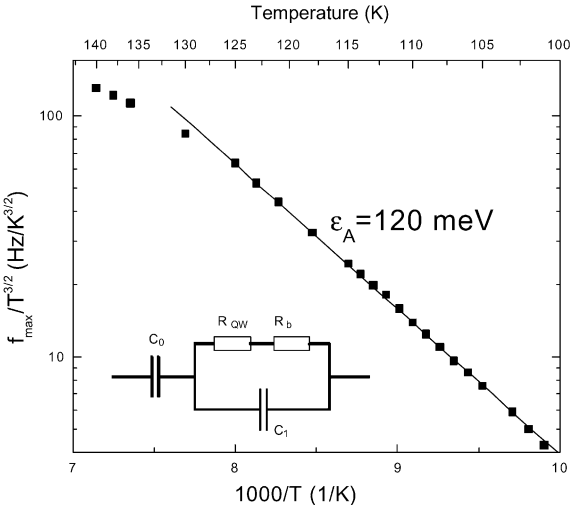

Fig. 6. Temperature dependence of the peak frequency. The slope of the $\log(f_{max}/T^{3/2})$ versus $1/T$ characteristics determine the activation energy for electron emission from the QWs into continuum. The inset shows the equivalent circuit of QWIP-LED.

$$C_0 = \varepsilon A/W, \tag{1}$$

$$C_1 = \varepsilon A/L, \tag{2}$$

$$R_b = \frac{L+W}{AL}\frac{1}{e\mu n}, \tag{3}$$

$$R_{QW} = R_b \times \frac{D/L}{v_{QW} - D/L + \sqrt{D_{\tau_c}}\coth(L/\lambda)}, \tag{4}$$

where L is the base thickness, e is the electron charge, μ is the mobility of the continuum state electrons, n is their concentration, $D = \mu kT/e$ is the diffusion coefficient, v_{QW} is the QW capture velocity [11], $\tau_c/L_p/v_{QW}$ is the QW capture time, and $\lambda = \sqrt{D_{\tau_c}}$ is the diffusion length.

The admittance of the equivalent model $Y(\omega) = G(\omega) + i\omega C(\omega)$ is given by the following formulas:

$$G(\omega)/\omega = \frac{\omega C_0^2 R}{1 + [\omega R(C_0 + C_1)]^2}, \tag{5}$$

$$C(\omega) = C_{HF} + \frac{C_{LH} - C_{HF}}{1 + [\omega R(C_0 + C_1)]^2}, \tag{6}$$

where $R = R_b + R_{QW}$, $C_{LF} = C_0$, and $C_{HF} = C_0C_1/(C_0 + C_1)$. Admittance normalized by angular frequency $G(\omega)/\omega$ and derivative of capacitance $dC/d(\log\omega)$ have peaks at frequency $\omega_m = 1/[R(C_0 + C_1)]$. Since the resistance R is a function of temperature $1/R \propto T^{3/2}\exp[-\varepsilon_a/(kT)]$ (ε_a is the activation energy of the QW), the value of the activation energy ε_a can be obtained by measuring the maximum frequency ω_m at various temperatures. The activation energy of the QW is related to the conduction band offset ΔE_c as $\varepsilon_a = \Delta E_c - \varepsilon_1 - \varepsilon_F$, where ε_1 is the ground state energy with respect to the bottom of the QW, $\varepsilon_F = kT\ln\left[\exp\left(\pi\hbar^2\Sigma/m_w kT\right) - 1\right]$ is the Fermi energy of electrons in the QW, Σ is the two-dimensional carrier concentration in the QW, and m_w is the carrier effective mass in the QW.

Fig. 5 shows the frequency dispersion of the capacitance and normalized conductance at various temperatures for voltage $V = -6$ V. The peak values of the normalized conductance are very close to each other in the temperature range 100–130 K. The values of the peak frequencies were found by Lorentzian fitting of $G(\omega)/\omega$ data. The peak frequency (normalized by $T^{3/2}$) is plotted on Fig. 6 as a function of the inverse temperature. The activation energy $\varepsilon_a = 120$ meV obtained by a linear fitting is attributed to thermionic emission of electrons from the QWs. This value agrees well with the activation energy extracted from the temperature dependence of the dark current I–V characteristics under forward bias conditions. The calculated ionization energy is $\varepsilon_i \approx 160$ meV, which gives the conduction band offset $\Delta E_c = 255$ meV. The corresponding Al mole fraction in the barriers is $x = \Delta E_c/0.8125$ meV ≈ 0.31. This value disagrees with the design parameter $x = 0.45$. The value $x = 0.45$ has been confirmed by the SIMS analysis of the QWIP-LED structures and by the infrared absorption spectroscopy data.

3. Conclusions

In conclusion, we have applied space charge spectroscopy to reverse biased QWIP-LED. The step-like behavior of the low-frequency capacitance caused by the discrete extension of the space charge region was used to determine the QW doping level, superlattice period, and the number of the QWs. Admittance measurements over a wide range of temperatures and frequencies showed the resonance behavior, which allowed the calculation of the activation energy of the QWs. The parameters of the QWIP-LED extracted from our measurements – QW doping density, period length, and number of periods – are in good agreement with the values of the design parameters. The extracted activation energy and conduction band offset disagree with the design parameters. Thus, we conclude, that the admittance spectroscopy data and dark I–V characteristics under forward bias are influenced by some unaccounted physical effects, such as defect-assisted tunneling from the QWs, which is probably due to a poor material quality of the present QWIP-LED samples with high Al mole fraction in QWIP barriers.

Acknowledgements

This work was supported in part by the NSF under grant #ECS-98-09746. The work at NRC was supported in part by DND. Work at CAU was supported by DOE grant no. DE-FG02-97 ER45647.

References

[1] V. Ryzhii, M. Ershov, M. Ryzhii, I. Khmyrova, Jpn. J. Appl. Phys. Part 2 34 (1995) L38.
[2] H.C. Liu, J. Li, Z.R. Wasilewski, M. Buchanan, Electron. Lett. 31 (1995) 832.
[3] M. Ershov, H.C. Liu, L.M. Schmitt, J. Appl. Phys. 82 (1997) 1446.
[4] H.C. Liu, L.B. Allard, M. Buchanan, Z.R. Wasilewski, Electron. Lett. 33 (1997) 379.
[5] L.B. Allard, H.C. Liu, M. Buchanan, Z.R. Wasilewski, Appl. Phys. Lett. 70 (1997) 2784.
[6] E. Dupont, H.C. Liu, M. Buchanan, Z.R. Wasilewski, D. St-Germain, P. Chevrette, Appl. Phys. Lett. 75 (1999) 563.
[7] E. Dupont, H.C. Liu, M. Buchanan, S. Chiu, M. Gao, Appl. Phys. Lett. 76 (2000) 4.
[8] S.M. Sze, Physics of Semiconductor Devices, Wiley, New York, 1981.
[9] D.L. Losee, J. Appl. Phys. 46 (1975) 2204.
[10] D.V. Lang, M.B. Panish, F. Capasso, J. Allam, R.A. Hamm, A.M. Sergent, W.T. Tsang, Appl. Phys. Lett. 50 (1987) 736.
[11] E. Rosencher, B. Vinter, F. Luc, L. Thibaudeau, P. Bois, J. Nagle, IEEE J. Quant. Electron. 30 (1994) 2875.
[12] A.G.U. Perera, V.G. Silvestrov, S.G. Matsik, H.C. Liu, M. Buchanan, Z.R. Wasilewski, M. Ershov, J. Appl. Phys. 83 (1998) 991.
[13] D.V. Lang, J. Appl. Phys. 45 (1974) 3023.
[14] F. Luc, E. Rosencher, P. Bois, Appl. Phys. Lett. 62 (1993) 2542.
[15] M. Ershov, H.C. Liu, L. Li, M. Buchanan, Z.R. Wasilewski, V. Ryzhii, Appl. Phys. Lett. 70 (1997) 1828.
[16] M. Ershov, H.C. Liu, L. Li, M. Buchanan, Z.R. Wasilewski, A.K. Jonsher, IEEE Trans. Electron. Dev. 45 (1998) 2196.
[17] M. Ershov, V. Ryzhii, K. Saito, J. Phys. D 28 (1995) 2118.
[18] V.Y. Aleshkin, B.N. Zvonkov, E.R. Lin'kova, A.V. Murel', Y.A. Romanov, Semiconductors 27 (1993) 504.
[19] M. Ershov, A. Shik, H. Ruda, unpublished.
[20] X. Letartre, D. Stievenard, M. Lannoo, D. Lippens, J. Appl. Phys. 68 (1990) 116.